AD-A191 641 APPLICATION OF PARTICLE SIMULATIONS TO THE NRL LASER EXPERIMENT(U) LOS ALAMOS NATIONAL LAB NM D WINSKE 10 DEC 87 LA-UR-87-4072 1/1

UNCLASSIFIED F/G 20/9 NL

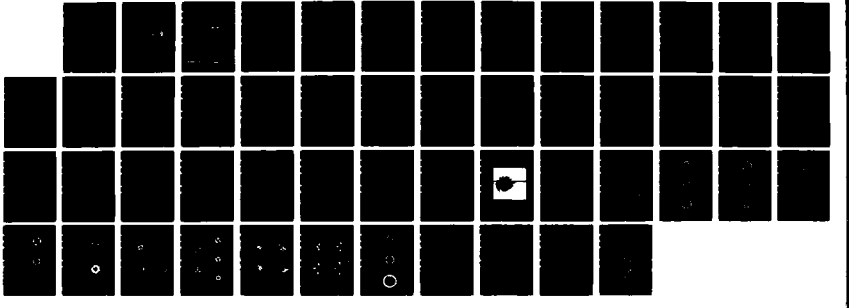

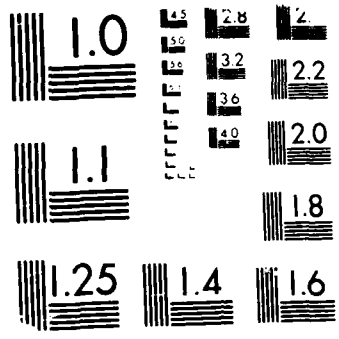

MICROCOPY RESOLUTION TEST CHART

LA-UR 87-4072

Los Alamos National Laboratory is operated by the University of California for the United States Department of Energy under contract W-7405-ENG-36

TITLE: APPLICATION OF PARTICLE SIMULATIONS TO THE NRL LASER EXPERIMENT

AUTHOR(S): Dan Winske, X-1

SUBMITTED TO: Report prepared for the Defense Nuclear Agency
under Project Code RB, Task Code RC, Work Unit 167

Los Alamos National Laboratory
Los Alamos, New Mexico 87545

FORM NO 836 R4
ST NO 2629 5/81

SECURITY CLASSIFICATION OF THIS PAGE

REPORT DOCUMENTATION PAGE

1a. REPORT SECURITY CLASSIFICATION UNCLASSIFIED	1b. RESTRICTIVE MARKINGS
2a. SECURITY CLASSIFICATION AUTHORITY	3. DISTRIBUTION / AVAILABILITY OF REPORT Approved for public release, distribution is unlimited
2b. DECLASSIFICATION / DOWNGRADING SCHEDULE	
4. PERFORMING ORGANIZATION REPORT NUMBER(S) LA UR 87-4072	5. MONITORING ORGANIZATION REPORT NUMBER(S)
6a. NAME OF PERFORMING ORGANIZATION Los Alamos National Lab 6b. OFFICE SYMBOL (If applicable) X-1	7a. NAME OF MONITORING ORGANIZATION
6c. ADDRESS (City, State, and ZIP Code) Los Alamos, New Mexico 87545	7b. ADDRESS (City, State, and ZIP Code)
8a. NAME OF FUNDING / SPONSORING ORGANIZATION Defense Nuclear Agency 8b. OFFICE SYMBOL (If applicable) RAAE	9. PROCUREMENT INSTRUMENT IDENTIFICATION NUMBER
8c. ADDRESS (City, State, and ZIP Code) Washington, DC 20305	10. SOURCE OF FUNDING NUMBERS PROGRAM ELEMENT NO. / PROJECT NO. / TASK NO. / WORK UNIT ACCESSION NO.

11. TITLE (Include Security Classification)
APPLICATION OF PARTICLE SIMULATIONS TO THE NRL LASER EXPERIMENT

12. PERSONAL AUTHOR(S) D. Winske

13a. TYPE OF REPORT	13b. TIME COVERED	14. DATE OF REPORT (Year, Month, Day)	15. PAGE COUNT
Technical	FROM 10/87 TO 12/87	87 Dec 10	45

16. SUPPLEMENTARY NOTATION
This work was supported by the Defense Nuclear Agency under Project Code RB, Task Code RC, Unit Work Code 167, Unit Work Title: Simulations and Modeling of HANE/VHANE.

17 COSATI CODES		
FIELD	GROUP	SUB-GROUP

18. SUBJECT TERMS (Continue on reverse if necessary and identify by block number)
Laser experiment, Flute instabilities
Early time structuring
Particle simulations

19. ABSTRACT (Continue on reverse if necessary and identify by block number)

Particle simulation methods are used to address issues related to recent results of the NRL laser experiment. The simulations, which include all the electron and ion scale lengths, examine dense plasma clouds expanding across a magnetic field into a vacuum under various conditions. The wavenumbers of the observed short wavelength instability, identified as the lower hybrid drift instability, are found to be independent of the magnetic field (in agreement with experiment) and the ion to electron mass ratio, consistent with a simple model for the expansion. In addition, differences in the instability due to the initial velocity distribution and the angular spread of the expansion are studied. Nonlinear phenomena, such as possible flute tip bifurcation, bending and separation, have also been observed in the calculations and are related to similar effects seen in the experiments. However, detailed analysis of the simulations show that there is no short wavelength cutoff to the instability, contrary to the predictions of linear theory, indicating that the wavelength scaling is spurious. Possible physical and numerical reasons for this behavior are examined, and it is shown that another instability, the electron cyclotron drift instability can still be excited at shorter wavelengths. The overall consequences of the results on the suitability of these methods for modeling the laser experiment are discussed.

20. DISTRIBUTION / AVAILABILITY OF ABSTRACT ☒ UNCLASSIFIED/UNLIMITED ☐ SAME AS RPT. ☐ DTIC USERS	21. ABSTRACT SECURITY CLASSIFICATION UNCLASSIFIED
22a. NAME OF RESPONSIBLE INDIVIDUAL Dan Winske	22b. TELEPHONE (Include Area Code) 505-667-2868 22c. OFFICE SYMBOL X-1

DD FORM 1473, 84 MAR 83 APR edition may be used until exhausted. All other editions are obsolete.

SECURITY CLASSIFICATION OF THIS PAGE

Application of Particle Simulations to the NRL Laser Experiment

Dan Winske

Los Alamos National Laboratory

Abstract

Particle simulation methods are used to address issues related to recent results of the NRL laser experiment. The simulations, which include all the electron and ion scale lengths, examine dense plasma clouds expanding across a magnetic field into a vacuum under various conditions. The wavenumbers of the observed short wavelength instability, identified as the lower hybrid drift instability, are found to be independent of the magnetic field (in agreement with experiment) and the ion to electron mass ratio, consistent with a simple model for the expansion. In addition, differences in the instability due to the initial velocity distribution and the angular spread of the expansion are studied. Nonlinear phenomena, such as possible flute tip bifurcation, bending and separation, have also been observed in the calculations and are related to similar effects seen in the experiments. However, detailed analysis of the simulations show that there is no short wavelength cutoff to the instability, contrary to the predictions of linear theory, indicating that the wavelength scaling is spurious. Possible physical and numerical reasons for this behavior are examined, and it is shown that another instability, the electron cyclotron drift instability can still be excited at shorter wavelengths. The overall consequences of the results on the suitability of these methods for modeling the laser experiment are discussed.

1. Introduction

Plasmas expanding (or being compressed) at subAlfvenic speeds perpendicular to a magnetic field develop flute instabilities at the plasma-magnetic field interface. The effect has been known for many years in theta-pinch implosions [Keilhacker *et al.*, 1974] and has also been observed in laser produced plasmas [Okada *et al.*, 1981]. More recently, the same phenomena has been seen in expanding barium clouds in the magnetotail [Bernhardt *et al.*, 1987] and in laser-plasma interactions [Ripin *et al.*, 1987]. In the laser experiments the flute structures exhibit very interesting behavior: the outer tips are freestreaming (i.e., not slowed down by the magnetic field), sometimes seem to bifurcate, and at late times often have a spiral pattern.

A theoretical explanation for the laser observations has been put forward by Huba *et al.* [1987], extending earlier work for the barium releases [Hassam and Huba, 1987]. On the basis of a modified set of MHD equations, they suggest that the instability which gives rise to the flutes is an unmagnetized ion Rayleigh-Taylor interchange mode that arises due to the slowing of the plasma as it expands against the magnetic field. The theory predicts a growth rate that increases linearly with k, the wavenumber, with $L_n^{1/2}$, L_n being the density scale length, and $g^{1/2}$, where g is the plasma deceleration. Alternatively, Winske [1987] has argued that the instability is the lower hybrid drift instability exhanced in the expanding plasma situation by the deceleration of the plasma. Earlier, Batchelor and Davidson [1975] had used the properties of the instability (claiming $g \simeq 0$) to explain the flute modes observed in theta-pinch compressions, while Okada *et al.* [1981] applied similar theory with $g \neq 0$ to interpret their laser experiments. Winske [1987] has shown that the long wavelength limit of the lower hybrid drift instability with deceleration [hereafter

referred to as the LHDI] reproduces the Hassam and Huba [1987] growth rate scaling. The maximum growth rate of the LHDI, however, occurs at very short wavelengths ($k\rho_e \sim 1$, ρ_e = electron gyroradius), which does not seem to explain the longer wavelengths observed in the barium release or the laser experiments. Other related linear theory calculations and simulations [Galvez *et al.*, 1987] have reached the same conclusion, although their simulations demonstrate good agreement between the structure wavelengths observed in their simulations and the wavelengths at maximum growth predicted by linear theory. It has been suggested that nonlocal, nonlinear, finite beta, or velocity shear effects may tend to inhibit the shortest, fastest growing modes from dominating at late times, but no conclusive studies have yet been carried out. However, until one understands the role of these short wavelength modes, simulations based on numerical models which ignore them [e.g., hybrid codes with massless electrons, or single fluid codes] are suspect.

In our previous report [Winske, 1987] we discussed in detail the linear and nonlinear theory for the LHDI and presented particle simulations of dense plasma clouds expanding into a tenuous background plasma. While a number of cases were run and briefly described, we concentrated there on one particular simulation and compared in detail the results of the calculations with theory. Reasonably good agreement was obtained, when the local parameters were well known. In this report we discuss a number of simulations that have been done and emphasize the differences in the results as various parameters are changed. We then try to understand the behavior of the instability under different conditions in terms of the theory of the LHDI. In conducting such studies one must keep in mind that the parameters are not all independent. For example, varying the ion to electron mass ratio affects not only the time scale for the instability ($\sim \omega_{LH}^{-1} \sim (m_e/m_i)^{1/2}$), but also changes

the magnetic confinement radius (R_B) as well as the deceleration rate. In addition to changing the mass ratio (with or without changing R_B), we have also varied the magnetic field strength (again with or without altering R_B), the initial velocity profile, and the angular spread of the expanding plasma. Furthermore, we have examined the direction in which the flutes bend and looked for their bifurcation at late times. Overall, the results seem to be in good qualitative, if not quantitative, agreement with the theory. We have also carried out a rather careful analysis of the simulations to see whether the shortest waves observed in the simulations are physical or numerical in origin. Unfortunately, we find that electron effects, which are included in the calculations and are expected to provide a minimum scale length, do not prevent even shorter wavelength modes from growing. Explanations based on both physics and numerics are invoked to interpret the results. The most likely explanation is that another instability, the electron cyclotron drift instability, remains unstable under most conditions of the simulation and is responsible for the observed short wavelength structures. The fact that the observed wavelengths scale with the grid size explains their lack of magnetic field or mass dependence.

The outline of this report is as follows. We briefly review the principal results of the laser experiments of Ripin *et al.* [1987] in Section 2 and of the theory of the LHDI in Section 3. The various simulations are described in Section 4 and interpreted in terms of the theory. Section 5 addresses numerical issues, and Section 6 summarizes the results. The overall conclusion is that the shortest wavelength modes which are determined by the numerical grid seem unavoidable, casting doubts on any scaling studies based on them. Given such restrictions, the best course of action seems to be the use of more macroscopic codes (e.g., hybrid methods) with a suitable resistivity algorithm, or some other numerical

trick, to try to flush out the initial perturbations so that they do not dominate at late times.

2. Review of the Results of the NRL Laser Experiment

The NRL laser experiments were conducted with a Nd-laser ($10^{13}W/cm^2, 30J$) onto a small Al disk target, producing a plasma mass of about 0.2 μgm, half of which expanded forward into a strong, 0.1-1.0 T magnetic field. The outer surface of the expanding plasma structures into field aligned (flute) modes, as was observed by means of a gated optical imager camera. Figure 1 [from Ripin *et al.*, unpublished] shows an example of the phenomena. This particular shot was taken at 99ns with B=1T at somewhat higher laser energy (367 J). One sees that the plasma has expanded from the target (left edge of the picture) rather symmetrically and the outer edge of the plasma has structured, producing finger-like projections which are fairly regular in shape. Other measurements indicate that the tips of the flutes are freestreaming, i.e., not slowed down by the magnetic field, although at late times the flutes acquire a curved shape, which is in the electron $\vec{E} \times \vec{B}$ or electron cyclotron sense of rotation. These is also a suggestion that the flutes bifurcate in time to maintain roughly constant wavelength, although the measurements are made at different times on different shots. The wavelength of the flute modes does not appear to be a function of the applied magnetic field. This is in contrast to the earlier Japanese experiments [Okada *et al.*, 1981] which showed that the wavenumber of the unstable modes scaled with the magnetic field, $\sim B^{0.8}$.

It should be noted that in these experiments the size of the plasma ($\sim R_B$) was comparable to the ion gyroradius, and much larger than the wavelength of the observed

structures. For example, for B=1T, R_B is about 3.3cm and ρ_i was estimated to be about 1.4cm, while at B=0.1T, $R_B \simeq$ 15cm, and $\rho_i \sim$ 14cm. Similarly, the time scale for the instability ($< 10^{-8}$ sec) was much less than the ion gyroperiod. It is interesting to note that the barium releases in the magnetotail [Bernhardt *et al.*, 1987] had much different physical dimensions and values for the parameters, but again $\lambda \ll \rho_i \sim R_B$. In both situations, as expected, the expanding plasma pushes out the magnetic field to form a diamagnetic cavity. Magnetic probe measurements on the laser experiment show that about 30% of the field is excluded within the plasma front. In both experiments high frequency electric field noise was also detected [Ripin *et al.*, 1987; Gurnett *et al.*, 1986]. Finally, the laser experiments also indicate that the onset of the instability (in time and/or distance from the target) was not a strong function of the applied magnetic field.

3. Review of Linear Theory of the LHDI

A detailed discussion of the lower hybrid drift instability in its generalized form is given in Winske [1987], where the linear dispersion equation is derived and numerous analytic and numerical solutions are presented. We restrict ourselves here to a few relevant features that will be needed to interpret the simulations.

The physical mechanism which gives rise to the instability is shown in Figure 2. For times short compared to an ion cyclotron period ($\Omega_i t < 1$), the ions can be taken as unmagnetized. As they expand radially outwards across the magnetic field, the ions are constrained by the electrons which are tied to the magnetic field. An electric field is then set up at the surface, which retards the ions and pulls out the electrons. In the radial direction, the expansion thus continues, with the electrons and ions being compressed into

a thin coupling shell. Azimuthally, the radial electric field drives the electrons via $\vec{E} \times \vec{B}$ relative to the ions, giving rise to the instability.

In order to derive a linear dispersion equation that describes the local properties of this azimuthally directed instability, one applies the response of the unmagnetized ions and the strongly magnetized electrons to perturbations in the θ direction. The effect of the radial expansion on the local dispersion equation enters only through the $\vec{E} \times \vec{B}$ drift velocity of the electrons. Generally, the radial electric field consists of two parts. One piece is due to the slowing of the plasma as it pushes against the magnetic field (characterized by a deceleration $g = -dV_r/dt$. The other piece is due to the density gradient ($\epsilon_n = -n_i dn_i/dr$), which is the dominant part when the plasma is not accelerating. Assuming for simplicity cold ($T_e = 0$) electrons, the radial electric field can be written as

$$eE_r = -m_i g - T_i \epsilon_n \tag{1}$$

where m_i=ion mass, T_i=ion temperature=$\frac{1}{2} m_i v_i^2$, so that the $\vec{E} \times \vec{B}$ velocity, V_E, in a magnetic field B_o is

$$V_E = -\frac{cE_r}{B_o} = \frac{m_i c g}{eB_o} + \frac{T_i c}{eB_o}\epsilon_n = V_g + V_n \tag{2}$$

The usual lower hybrid drift instability corresponds to $V_g = 0$; the plasma expansion in both the laser and the simulations to be described later is characterized by $V_g \gg V_n$. In electrostatic simulations, e.g., Galvez *et al.* [1987], the part of the electric field characterized by g is not a consequence of compressing the magnetic field, but rather results from charge separation. A simple model for g in this situation has yet to be derived, but it can be shown from the simulations that $V_g \sim V_n$.

Proceeding in the usual fashion, the linear dispersion equation can be derived [Winske,

1987]. It is not written down here, as by itself it is not very revealing. Analytical approximations can be obtained in various limits, however, which are more useful here. Generally, unstable solutions occur for $0 \leq k \leq k_1$. For $k \sim 0$ (long wavelength limit), the growth rate (γ) scaling can be shown to that of Hassam and Huba [1987], and ω_r, the real frequency, is very small. Maximum growth of the instability, however, occurs at much shorter wavelength, $k \simeq k_m < k_1$. There is some question at present whether the modes with maximum growth rate are relevant to either the laser experiment or other situations, such as AMPTE. They are, however, excited and are important in the simulations, if sufficient resolution exists for their occurrence. In this report we shall be primarily concerned with the waves of maximum growth and how they scale, and unless otherwise noted, "by comparing with linear theory" we will mean "by comparing with linear theory for the fastest growing waves". The fastest growing modes are also characterized by $\omega_r \sim \gamma \sim \omega_{LH}$. The fact that the structures observed in the laser experiments (and the barium releases) show little azimuthal movement suggests $\omega_r \sim 0$. This might indicate that the flute modes seen in the experiments have become nonlinear with properties much different than they possesses at earlier time, or that hardier, low frequency (and longer wavelength) modes have taken over at later time. In the simulations, the mode number is roughly constant and the modes appear to have a larger frequency at early times, suggesting a nonlinear frequency shift occurs later, as happens for the usual lower hybrid drift instability without deceleration [Winske and Liewer, 1987]. Nevertheless, comparison with the strongest linearly growing modes seems a good place to start.

The linear dispersion equation yields the following solutions for the most unstable

modes:

$$k^2 L_i^2 = \frac{(m_i/m_e)\epsilon_n L_i}{V_E/v_A} \tag{3}$$

$$\frac{\omega}{\Omega_i} = \frac{(V_E/v_A)^{2/3} k L_i}{(V_E/v_A + \epsilon_n L_i)^{1/3}} \left(\frac{1+i\sqrt{3}}{2}\right) \tag{4}$$

where $L_i = c/\omega_i$, $\Omega_i = eB_o/m_i c$, and v_A = Alfven speed.

When $V_g \ll V_n$, these equations simplify to

$$\frac{k v_i}{\omega_{LH}} = \sqrt{2}(1 - V_g/2V_n) \tag{5}$$

$$\frac{\omega}{\omega_{LH}} = \frac{(\epsilon_n v_i/\Omega_i)^{1/3}(1+i\sqrt{3})}{2^{7/6}(1+\beta_i/2)^{1/3}} \left(1 + \frac{2V_g}{3V_n}\right) \tag{6}$$

where $\omega_{LH} = \omega_i/(1+\omega_e^2/\Omega_e^2)^{1/2}$ is the lower hybrid frequency, and $\beta_i = 8\pi n T_i/B_o^2$. For $V_g = 0$, this reduces to the well known results for the usual lower hybrid drift instability; when $V_g \neq 0$, the presence of the deceleration decreases k and increases ω_r and γ.

For $V_g \gg V_n$, Equations (3) and (4) reduce to

$$k = \omega_{LH}(\epsilon_n/g)^{1/2} \tag{7}$$

$$\frac{\omega}{\omega_{LH}} = \frac{(\epsilon_n L_i)^{1/2}}{(V_g/v_A)^{1/6}} \frac{1+i\sqrt{3}}{2} \tag{8}$$

Again, increasing g reduces k (increases the wavelength), but now tends to reduce ω_r and γ. Numerical solutions of the complete dispersion equation show good quantitative agreement with (5) and (6) and at least qualitative agreement with (7) and (8).

While these results are interesting, in order to compare later with the simulations, they need to be expressed somewhat differently. In the simulation we will vary ω_e/Ω_e and m_i/m_e and see how the mode number or wavenumber (i.e., k) and the growth time ($\sim \gamma^{-1}$) change. Equations (7) and (8) then give

$$\frac{kc}{\omega_e} = c\left(\frac{m_e}{m_i}\right)^{1/2}\left(\frac{\Omega_e}{\omega_e}\right)\left(\frac{\epsilon_n}{g}\right)^{1/2} \tag{9}$$

$$\frac{\gamma}{\omega_e} = \frac{\sqrt{3}}{2}(\frac{m_e}{m_i})^{1/2}(\frac{\Omega_e}{\omega_e})\frac{(\epsilon_n L_i)^{1/2}}{(V_g v_A)^{1/6}} \tag{10}$$

where $\omega_{LH} \simeq (\Omega_e \Omega_i)^{1/2}$ for $\omega_e^2/\Omega_e^2 \gg 1$, and we have expressed k and γ in terms of ω_e, the plasma frequency, because this is the normalizing quantity in the simulations. These results demonstrate a clear dependence for both γ and k on ω_e/Ω_e and m_i/m_e.

However, we have yet to relate g to other parameters. This is more important for (9) than (10), because of the very weak dependence on V_g in (10). The deceleration g can be related to other parameters assuming radial pressure balance [Huba, 1987]. In two dimensions this can be expressed as

$$\frac{1}{2}Nm_iV_D^2 = \frac{1}{2}Nm_iv_r^2 + \frac{B_o^2}{8\pi}r^2\pi L \tag{11}$$

where N is the number of cloud ions = $n_c\pi r_o^2 L$ (r_o = initial cloud radius, n_c=initial cloud density, L= scale length in third (z) direction). Maximum g occurs at the end of the expansion, where $v_r = 0$ and $r = R_B$, the magnetic confinement radius:

$$\frac{1}{2}Nm_iV_D^2 = \frac{B_o^2}{8\pi}R_B^2\pi L \tag{12}$$

$$g = -\frac{dv_r}{dt} = \frac{V_D^2}{R_B} \tag{13}$$

$$g = V_D\ \frac{c}{r_o}\ \frac{\Omega_i}{\omega_c} \tag{14}$$

where $\omega_i^2 = 4\pi n_c e^2/m_i$. Thus,

$$\frac{kc}{\omega_e} \sim (\frac{\epsilon_n r_o c}{V_D})^{1/2}(\frac{\Omega_e}{\omega_e})^{1/2}(\frac{m_e}{m_i})^{1/4} \tag{15}$$

which indicates a weaker dependence on both m_i/m_e and ω_e/Ω_e than is implied by (9).

The difficulty with this approach is that the instability forms at early times, long before the plasma reaches R_B. This suggests another model, which leads to a different

scaling. Assume at early times that the ions stream ahead of the electrons a small distance Δ_r and exclude the magnetic field. Pressure balance is maintained by the electric field E_r set up in the process (ignoring the ion pressure contribution):

$$\frac{E_r^2}{8\pi} \simeq \frac{B_o^2}{8\pi} \tag{16}$$

However, Poisson's equation implies

$$\frac{dE_r}{dr} = -4\pi e\hat{n} = \frac{E_r}{\Delta_r} \tag{17}$$

where $\hat{n}$ is the ion charge density in the layer, or

$$eE_r = -B_o^2/4\pi\hat{n}\Delta_r \tag{18}$$

Since (1) implies $g \simeq -eE_r/m_i$, (9) becomes

$$\frac{kc}{\omega_e} \sim \frac{\hat{n}}{n} \tag{19}$$

independent of both ω_e/Ω_e and m_i/m_e. Thus, various scaling for the wavevector are possible, depending on the assumed physics of the expansion.

4. Simulations

This section consists of three parts. Part A is an overview of the simulations, reviewing previous work and describing the methods. In Part B numerous simulations in which the initial parameters are varied are discussed, and the results are interpreted in terms of the theory previously presented. Part C considers other issues important to the laser experiment, such as the late time behavior of the flutes.

A. Overview

The simulations are similar to those discussed in Winske [1987]. They were done with the fully electromagnetic, two-dimensional particle code WAVE. The principal difference is that here there is no (hot) background plasma. A dense plasma cloud (typically $n_c/n_o = 25$, radius $r_o = c/\omega_e$) expands at $V_D = v_A$ ($v_A^2 = B_o^2/4\pi n_o m_i$) outward against a uniform magnetic field B_o, which is in the z direction perpendicular to the expansion. Here n_o is the reference density that defines the system size, typically $L_x = L_y = 25c/\omega_e$, where $\omega_e^2 = 4\pi n_o e^2/m_e$, with the magnetic field given in terms of $\Omega_e/\omega_e = eB_o/m_e c\omega_e$ (typically $\Omega_e/\omega_e = 0.2$). Usually 125^2 cells are used to represent the system, and 40000 ions and electrons describe the expanding plasma. Nominal parameters include: $m_i/m_e = 100$, $v_i/c = 0.001$, and $v_e/c = 0.01$, with $V_D = 0.02c$. The choice of these values represents a compromise: one must keep the system size reasonable, yet resolve scales of interest. We thus tolerate some numerical heating of the electrons early in the simulation (since $\lambda_{De} < \Delta$); previously this was minimized with the addition of a hot background component. Elimination of the background does not change the results significantly, as will be shown later, and speeds up the calculations considerably. Finally, we note that in contrast to the calculations here, the simulations of Galvez *et al.* [1987] are electrostatic and involve the

thermal expansion of hot, large (many ion gyroradii) plasmas.

An example of one such simulation, with the nominal parameters given above, is shown in Figure 3. Displayed are the ions in real space (x-y) at various times [in the figures $\omega_{LH}t = (\Omega_e\Omega_i)^{1/2}t$]. At early time the outer edge of the expanding cloud is slowed by the magnetic field, while the inner edge is not, compressing the cloud into a thin "coupling shell". At somewhat later time, modes appear on the surface. The waves continue to grow as the plasma expands and eventually the plasma diffuses through the magnetic field. Compared to the case with a background plasma present [Figure 11, Winske (1987)], there is little difference in the size or shape of the expanding cloud. The modes in the present simulation are somewhat more diffuse and of slightly shorter wavelength (higher mode number m), but overall the differences are minor.

B. Parameter Variation

We next compare the results of various simulations in which some of the input parameters are varied. Without doing detailed comparisons of each case with linear theory (which requires accurate local measurements of quantities such as the relative electron-ion drift speed), we will attempt to interpret the results in terms of theory and relate, where possible, to the experimental results. Generally, the parameters will be varied about the "Standard Case" described in the previous subsection and snapshots of the ion density contours at a particular time rather than a sequence of plots will be shown.

The first case considers variation with ion mass, m_i/m_e, the other parameters kept constant. The results are shown in Figure 4: top panel, $m_i/m_e = 25$ at $\omega_e t = 175$; middle panel, standard case, $m_i/m_e = 100$, $\omega_e t = 225$; bottom panel, $m_i/m_e = 400$, at $\omega_e t = 300$. The times are chosen so that the instability is at about the same stage of development in

each case. It is clear that the heavier ion mass implies that the instability develops more slowly (in terms of clock time, i.e., $\omega_e t$) so that the size of the plasma shell is larger and the mode number m is larger. However, the wavenumber in the three cases is not much different, $ck/\omega_e (= 2\pi/\lambda) = 4.9, 3.9, 4.0$, respectively for $m_i/m_e = 25, 100, 400$, and given the difficulty in counting the modes, the results suggest that there is no mass dependence on the wavenumber. Note that expressing the time in terms of ω_{LH} [$\sim (\Omega_e \Omega_i)^{1/2}$], the three frames in Figure 4 correspond to $\omega_{LH} t = 7, 4.5, 3$. [One cannot say, however, how the actual growth rates vary in the simulations by just looking at these plots, since the time over which there is strong exponential growth of the waves is very limited, e.g., see Figure 15 in Winske (1987)]. As noted in the previous section, the wavenumber may have a rather strong $(m_i/m_e)^{1/2}$ dependence on mass, moderate dependence $(m_i/m_e)^{1/4}$, or no dependence, depending on conditions and the physics model assumed. Thus, the simulations are consistent with theory, assuming (16)-(19) is correct. An alternative possibility to be kept in mind, which is discussed in detail in the next section, is that the mode structure is instead limited by the spatial resolution of the grid; i.e., the maximum wavelength is $k \sim 1/\Delta x \sim 5\omega_e/c$.

In similar fashion, results showing the variation of Ω_e/ω_e are displayed in Figure 5: top panel, $\Omega_e/\omega_e = 0.1$ at $\omega_e t = 300$; middle panel, $\Omega_e/\omega_e = 0.2$ at $\omega_e t = 225$, the standard case; bottom panel, $\Omega_e/\omega_e = 0.4$ at $\omega_e t = 175$. Again, the ion density contours are shown at a comparable stage of development of the instability. As before, in terms of normalized time, the times are reversed, with the top panel actually being earliest ($\omega_{LH} t = 3$) compared to the other cases ($\omega_{LH} t = 4.5$ and 7, respectively). At larger values of Ω_e/ω_e the instability develops faster, hence the plasma has a smaller

radius and mode number. Again, $kc/\omega_e = 3.8, 4.0, 4.4$ for the cases $\Omega_e/\omega_e = 0.1, 0.2, 0.4$, respectively. As with the mass dependence, linear theory for Ω_e/ω_e variations predicts difference dependences in different regimes. Again, the estimate of k based on assuming a charge separation layer (16-19) gives no Ω_e/ω_e dependence. In contrast, in the simulations of Galvez *et al.* [1987], which have $g \sim 0$, the wavenumbers scale like Eq. (5). One recalls from the experimental results, that there is also some ambiguity. Ripin *et al.* [1987] indicate no variation of wavelength with B (i.e., Ω_e/ω_e), consistent with Eqs. (16)-(19), while Okada *et al.*, [1981] report $k \sim B^{0.8}$, consistent with (11)-(15). Again the differences may suggest the two experiments are run in different regimes. For example, the modes in Okada's experiment occur at maximum expansion [consistent with (11-15)], while in Ripin's experiment, the structures appear earlier, more like (16)-(19).

In order to further check the scaling and to normalize the differences, we have also done simulations in which R_B is kept constant. For example, in Figure 6 we have varied both m_i/m_e and Ω_e/ω_e together: top panel, $\Omega_e/\omega_e = 0.1$, $m_i/m_e = 25$; middle panel, $\Omega_e/\omega_e = 0.2$, $m_i/m_e = 100$, standard case; bottom panel, $\Omega_e/\omega_e = 0.4$, $m_i/m_e = 400$. In each case ω_{LH} is identical, with the results at $\omega_e t = 300$, $\omega_{LH} t = 6$. In this case, the size of the clouds are comparable ($\sim R_B$), the instability is about in the same state of development, and the mode numbers are roughly the same. This result is consistent with both the scaling (15) and (19).

Another way to compare the simulations is to vary Ω_e/ω_e and V_D/c to again keep R_B constant. Figure 7 displays the ion density contours for three cases all at $\omega_{LH} t = 6$: top panel, $\Omega_e/\omega_e = 0.1$, $V_D/c = 0.01$; middle panel, $\Omega_e/\omega_e = 0.2$, $V_D/c = 0.02$, standard case; bottom panel, $\Omega_e/\omega_e = 0.4$,$V_D/c = 0.04$. Again, the instability has developed to about

the same point (the top panel looks weaker, but may indicate a lower saturation level), the size of the plasmas, and the wavelengths are comparable in all cases. Again, the results are consistent with both (15) and (19).

The effect of varying the initial conditions has also been investigated. Figure 8 shows the standard case in which all the particles have the same initial radial velocity V_D and a second case where a self-similar initial radial velocity ($\sqrt{2}V_D r/r_o$) distribution was used. [The $\sqrt{2}$ is included so that the total kinetic energy is the same in each distribution.] The figure shows that both cases give similar results, about the same mode number and level of charge bunching. Because of the velocity spread, however, some ions remain behind in the expansion in the self-similar case, and at later times, it spreads to larger radius.

The initial angular spread of the expansion has also been varied. Figure 9 displays three self-similar initial distributions ($V_r = V_D r/r_o$) with angular spread $\pm\theta_o$ ($180^o, 90^o, 45^o$) and one $V_r = V_D$ case with $\theta_o = 90^o$, all at $\omega_e t = 300$. The three self-similar cases show some variation with θ_o: large θ_o gives a slightly longer wavelength and the flutes are somewhat more elongated. Both effects could be caused by the larger deceleration expected when θ_o is larger. Also note in the partial shells that the instability is also present on the rear side of the expansion at about the same wavelength. In this case the density gradient drift is very small, as the ion thermal speed is negligible, and the deceleration drift is about the same as on both sides of the shell. Finally, the bottom panel shows the constant initial velocity case with $\theta_o = 90^o$. Three effects are interesting: (1) there is little slowing of the shell, (2) the waves that form on the surface are quite small, and (3) the entire shell has rotated slightly in the counterclockwise direction. Because the ions are unmagnetized, this rotation must result from the ions following the electrons, which gives the correct sense.

The fact that there is little deceleration probably results from the fact that little B field get excluded; the flux can just flow around the shell. The small deceleration could imply smaller growth of the instability and lower saturation level [cf., Winske (1987) for the case of expansion in a slab geometry].

C. Other Issues

Besides demonstrating the growth of the instability, the laser experiments of Ripin *et al.* 1987] exhibited very interesting late time behavior, including the bifurcation of the flutes and their bending in time. The issue of whether the freestreaming flute tips can break off and continue propagating across the magnetic field is also important for the VHANE situation. Generally, the simulations [Winske, 1987] show that by the time the flutes are visible in real space, wave growth has saturated. Thus, much of what is observed is nonlinear phenomena that is not described by the theory presented earlier. More work, both experimental and theoretical, will be needed to understand the observations. The results discussed here are included to demonstrate that the particle simulations can be useful for these studies, although hybrid (massless, fluid electrons) [e.g., Brecht and Thomas, unpublished] will be better because of the larger spatial and temporal scales that can be used.

The top panel of Figure 10 shows the ion density contours for a run presented earlier [Figure 5, bottom panel] at later time. The Y-shaped structure at the top of the figure suggests a bifurcated flute mode. The lower panels show snapshots of the density at earlier times, in reverse order. It is clear from these pictures that the flute tip does not split, but that the modes just evolve in time, and the mode number remains pretty much unchanged. Similarly, comparing the middle panel of Figure 4 with the top panel of Figure 8 (i.e., the

standard case at two times) basically shows that the mode number does not change very much. Sometimes, e.g. the bottom panel of Figure 7, the contour plotter groups together two smaller, separate peaks into one larger structure. Overall, the constancy of the mode number is consistent with older simulations of the lower hybrid drift instability in slab geometry [Winske and Liewer, 1978] as well as recent mode coupling theory [Drake *et al.*, 1984]. A difference here, however, is the continuous expansion of the plasma allows the waves to be driven to higher amplitudes where stochastic-like decoupling of the electrons from the magnetic field [Drake and Lee, 1981] occurs. Thus, the electron behavior of the usual mode coupling model that involves ∇B resonaces may be expected to be modified.

Another interesting feature of Figure 10 is the direction that the flutes bend. Except for the Y-shaped structures, the arms generally spiral clockwise, i.e., in the ion sense of rotation (recall the B field is outward). This is characteristic of most of the simulations, e.g., Figure 3. The behavior is not due to ion gyromotion, because the ions are unmagnetized in the simulations. From examining the temporal sequence in Figure 10, it is evident that these curved arms are all rotating at a slow rate in the electron (counterclockwise) sense. One expects the arms to bend clockwise if the ends of the arms are just moving outward, but the bases rotate counterclockwise as the plasma there is carried by the waves which have phase velocities in the $\vec{E} \times \vec{B}$ (counterclockwise) direction. At early times, $\omega_r \sim \omega_{LH}$ but the waves do not affect the particles yet, while at late times the waves experience a nonlinear phase shift so that $\omega_r \ll \omega_{LH}$.

Although this is a reasonable interpretation, Figure 11 shows another case where the arms spiral in the electron sense of rotation. This case is characterized by a very rapid growth of the instability ($\Omega_e/\omega_e = 0.4$ and $n_c/n_o = 100$), which clumps the density at very

early times and then a continued, unconfined expansion across the magnetic field ensues.

Finally, Figure 12 shows another dense plasma ($n_c/n_o = 100, r_o = 2c/\omega_e$) expansion into a weak ($\Omega_e/\omega_e = 0.1$) field. In this case strong density bunches are formed at early time. Again, here there is not much confinement of the plasma. The rapid growth of the plasma waves to large amplitude allows the plasma to stream through the field. The interesting aspect of this example is that the density clumps, once formed, do not diffuse. Instead, the plasma propagates across the field as discrete plasmoids. While one has to be cautious in interpreting the simulation results, because artificial parameters (m_i/m_e, Ω_e/ω_e, etc) allow the wave turbulence and hence the anomalous resistivity (diffusion) to be artifically large, it does suggest that interesting behavior can occur under some conditions.

5. Analysis

In the previous section it was suggested that the lack of ion mass or magnetic field strength dependence of the wavenumber of the observed flute modes was not physical and instead related to numerical issues. Here we examine this question in some detail and conclude that the modes in the simulation are always determined by the grid size. However, the modes are physical and are likely due to a shorter wavelength instability, the electron cyclotron drift instability. The consequences of this result are discussed in the conclusions.

Previous simulations of plasma expanding across magnetic fields in which electron effects were ignored [Shonk and Morse, 1968; Brecht and Thomas, unpublished, 1987; Huba *et al.*, 1987] all indicated that the shortest allowable modes grow fastest. This is consistent with linear theory for the lower hybrid drift instability (or equivalently the

theory for the unmagnetized ion Rayleigh Taylor instability [Hassam and Huba, 1987]) in that at long wavelengths, $\gamma \sim k$. However, when electrons are included in the analysis, a sharp maximum in the growth rate curve, given by (3), occurs; at larger k, growth falls rapidly to zero. One thus expects that simulations which include full electron dynamics would show that modes at wavelengths shorter than this cutoff to be suppressed. This can be easily checked by varying the grid spacing in the simulation. Figure 13 shows the results of this test for the Standard Case of Figure 3 for three different grid spacings: (A) $\Delta = 0.125c/\omega_e$, (B) $\Delta = 0.0625$, and (C) $\Delta = 0.03125$ (in Figure 3, $\Delta = 0.2$). In each case we have kept the number of simulation particles the same and varied only the size of the simulation region; thus cases with smaller Δ were run a shorter time. The figure demonstrates clearly that more modes appear as the cell size shrinks and that the *shortest modes continue to dominate. Also, the waves tend to appear at earlier times.* Unfortunately, we are unable to continue the fine mesh runs in time without rezoning, which would then suppress the shortest wavelengths.

Several explanations for this behavior are possible. The first possibility is that the plasma properties change with grid size. For example, the magnitude of the radial electric field, and hence V_E, could depend on Δ [i.e., $\Delta \sim \Delta_r$ in (19)]; the unstable waves then correspond to the same instability, but under different conditions. In order to check this, we have examined the magnitude of the cross field drift and the properties of the modes expected from linear theory. The results are presented in Table 1. Generally, the results show that the cross-field drift speed is about the same in each case at the same time. Here V_E is determined from both narrow slices in x and y of the electron j_x and j_y and the density, as well as from V_θ versus θ phase space for the electrons. This result rules

out an electric field that depends on Δ . The magnitude of the electric field fluctuations increases as Δ decreases, but that it likely due to the fact that the number of particles per cell is decreasing. The radial electric field also increases with time. The magnitude of E_r and its variation with time is consistent with the simple model of the exclusion of the magnetic field [Huba, 1987], as shown in our earlier study [Winske, 1987]. Thus, for each run the magnitude of V_g increases with time, which according to linear theory, means that k is decreased. However, the plasma radius increases with time so that the mode number m=kr stays roughly constant, consistent with the simulations. For the case with the largest cell size, the dominant mode predicted by linear theory is roughly the same as that assuming the shortest modes dominate (i.e., $k_m \sim 1/\Delta$), but for the smaller Δ cases there is a clear separation between the mode number predicted by theory and that observed in the simulations.

The discrepancy between simulation and theory can be due to either numerical or physical reasons. So a second explanation is that the results are merely numerical, due to trying to simulate an initially round plasma on a square grid. Because the two can never match completely, there will always be short wavelength ($k \sim 1/\Delta$) perturbations [Brecht, private communication]. A counter argument to this is that such perturbations are expected to be strongly damped, according to the linear theory. The resolution of this issue awaits the development of an r-θ PIC code with variable spacing in the radial direction, which we hope to have running sometime next year.

A third explanation based on physical considerations primarily concerns whether there are shorter wavelength modes which can grow. A likely candidate is the electron cyclotron drift instability [ECDI] [Forslund *et al.*, 1970], which is another mode driven by the cross

field drift of the electrons relative to the ions. This instability occurs at higher frequency that the lower hybrid drift instability and involves the interaction of ion waves with electron Bernstein modes, i.e., $\omega \sim n\Omega_e, n = 1, 2, 3....$ The instability is known to be strong when $V_E \sim v_e$, the situation in the simulation; moreover, it is characterized by short wavelengths $k\rho_e \gg 1$. In Figure 14 we display solutions of the linear dispersion relation for the LHDI ($T_e = 0$) and the ECDI for the simulation parameters of Table 1 at $\omega_e t = 25$. Only the two lowest branches of the ECDI are shown. Maximum growth ($\gamma_m \sim 0.047\omega_e$) occurs at much larger k ($kc/\omega_e \sim 160$), with the instability persisting for even much larger values of k (higher n). At higher mode numbers the γ verus k curves broaden so that eventually the unstable bands overlap. The large gap between the LHDI and the n=1 branch of the ECDI decreases when finite electron temperature effects are included in the LHDI dispersion relation. The conclusion fron this graph is that there are real, short wavelength unstable linear modes which can grow.

The principal difficulty is whether such unstable waves can grow to significant amplitude. Generally, the ECDI is dismissed as being unimportant [Lampe *et al.*, 1972] because it saturates at low amplitudes. This is because the instability depends on the cyclotron resonances of the electrons and magnetic field fluctuations or gradients tend to destroy the resonances whenever the instability grows to even small amplitudes. However, because of the persistence of the electric field in time, the instability may be driven to larger amplitudes than expected, just as the LHDI is driven to levels far exceeding the ion trapping limit usually expected, in this expanding geometry [Winske, 1987]. The ECDI (and the LHDI to a lesser extent) is suppressed when $k_{||} \neq 0$ [Lashmore-Davies and Martin, 1973]. Simulations with the magnetic field tilted so that $B_x \neq 0$, however, show no real differ-

ence. This lack of stabilization may be an artifact of the two-dimensional nature of the simulation, similar to the observed lack of shear stabilization of the LHDI. Alternatively, the finite $k_{||}$ stabilization may be removed when electromagnetic effects are included, as happens when the instability involves ion resonances [Brecht, 1982].

Finally, one asks whether there are regimes where the shortest wavelengths can be resolved. Clearly, if one starts with large plasmas ($r_o \gg \rho_i \sim R_B$), the most unstable modes are well resolved [Galvez *et al.*, 1987]. However, for the laser case, one wants to study the opposite situation, where $r_o \ll \rho \sim R_B$. While one can have reasonable parameters in terms of ion quantities, e.g., $V_D \sim v_A$, $r_o \ll \rho_i$, because of the compression of scales by choosing ω_e/Ω_e and m_i/m_e small, one is always in a regime where V_E is not negligible compared to v_e and the electron cyclotron drift instability always seems to occur. For example, increasing T_e/T_i while reducing V_E/v_e does not improve the situation very much.

6. Conclusions

In summary, in this report we have described results from a number of particle simulations of dense plasmas expanding at the Alfven speed into a vacuum across a strong magnetic field. This type of configuration is subject to a strong instability that produces flute modes on the outer surface of the expanding plasma. Such effects have been observed and investigated in laser produced plasmas [Ripin *et al.*, 1987] and in barium releases in space [Bernhardt *et al.*, 1987], and have been the subject of much recent theoretical work [Hassam and Huba, 1987; Huba *et al.*, 1987; Winske, 1987; Galvez *et al.*, 1987]. Our previous report [Winske, 1987] suggested that the lower hybrid drift instability enhanced

by the deceleration of the plasma across the magnetic field was a good candidate to explain the observations, although there was considerable disagreement between the observed wavelengths and those corresponding to the fastest growing waves of linear theory.

Our purpose here has been to describe numerous simulations, varying the initial conditions in a systematic fashion to understand the scaling of the instability with various parameters and to compare with theoretical predictions. Because of the interconnection of the input conditions through the deceleration process, such scaling studies are not trivial. We have varied both the mass ratio and the magnetic field strength (Ω_e/ω_e) independently, in which case the size of the plasma varies, as well as with other parameters so that $R_B \simeq$constant. It has been shown that the wavelength of the instability is independent of these two quantities, contrary to the standard theory in which the deceleration is related to the compression of the magnetic field. A closer examination of the results and the simulation methods suggest that the magnitude and time variation of the electric field based on the magnetic field compression model is basically correct. The wavelength of the instability, however, is always determined by the grid size. For wavelengths shorter than those predicted by the lower hybrid drift instability, unstable modes that can be identified with the electron cyclotron drift instability persist.

Given the limitation of the minimum wavelength due to grid effects, we have nevertheless also shown some variation in the character of the instability with the initial distribution in radial velocity and angular spread. We have seen, for example, that partial shells with self-similar velocity distributions structure on the inner edge with about the same properties as on the outer edge, but partial shells with constant intial velocity distributions do not seem to structure at all. In addition, a number of late time (probably nonlinear)

effects have been observed in the simulations that are relevant to the experiment. First, we have shown that the tips of the flute modes which appear to bifurcate are actually closely spaced waves that are diverging. Overall, there seems to be little tendency for the waves to cascade to longer or shorter wavelengths in the simulations, at least on the time scale studied. Exceptions to this rule are cases where very strong instabilities are excited and dynamic, nonlinear processes (bending or breaking off of the flute tips) are seen. We have observed flute tips that bend in the electron sense of rotation in the magnetic field (like the experiment) as well as in the ion sense.

The work included in this report constitutes a preliminary study of the basic physics that should occur in the laser experiment. So far, it has been primarily a test of the capabilities and the limitations of the simulations and the linear theory to explain them. And it has pointed out areas of nonlinear physics that need further study to explain the data. Furthermore, it has demonstrated the difficulties of improving the numerical modeling of both the laser configuration and the AMPTE barium releases.

The overall conclusion of this study points to a fundamental limitation in using particle methods to model the laser experiments. The original purpose of employing a simulation model with full electron and ion dynamics, which sacrifices some reality by compressing ion and electron scales, was to estimate the importance of the electrons is limiting short wavelength fluctations. However, a detailed analysis of the simulations demonstrate that beyond the shortest wavelengths allowed by the lower hybrid drift instability, other unstable modes due to the electron cyclotron drift instability persist down to the shortest scales realizeable. The simulations thus suggest that the shortest wavelengths in any reasonable sized simulation will be dominated by numerical grid effects. On the positive side, the

simulations do show that there are short wavelength modes present, even at very early times, which heat the plasma and diffuse it through the magnetic field. The radial electric field that is set up and tends to increase in time has been shown to be consistent with the simple model of magnetic field exclusion, and is itself not dependent on the grid size. Because of the continued deceleration of the plasma by the magnetic field, the azimuthal current is not able to relax, and hence the instability can be driven to rather high levels. The net effect is that one gets a rather broad (c/ω_i), turbulent boundary layer where the initial waves which brought this about should be washed away. Longer wavelength, slower growing modes may then develop at the surface of this broadened layer.

Given the fact that the dominant modes in the simulation at early times at determined numerically (which by judicious choice of the grid can be chosen to be those expected from linear theory), one would like to run the simulation long enough until they are no longer dominant. With the full particle code that follows electron scales that is generally not possible, although some of the runs with a very violent instability initially (e.g., Figures 11 and 12) show this behavior. A better approach would be hybrid calculations [e.g., Brecht and Thomas, unpublished] where by means of a time varying resistivity it might be possible to flush out the initial perturbations and then let longer wavelength modes develop. This washing out of the system at early times apparently happens in the experiments and may explain why the observed structures seem independent of the magnetic field and exhibit peculiar nonlinear behavior.

Acknowledgements

We acknowledge useful and stimulating discussions with Drs. K. Akimoto, S. H.

Brecht, S. P. Gary, K. Quest, B. H. Ripin, and V. A. Thomas. This work was performed under the auspices of the U. S. Department of Energy, and was supported by the Defense Nuclear Agency under Project Code RB, Task Code RC, Work Unit Code 167, and Work Unit Title "Simulations and Modeling of HANE/VHANE."

References

Batchelor, D. B., and R. C. Davidson, Nonlocal analysis of the lower hybrid drift instability in theta-pinch plasmas, *Phys. Fluids, 19*, 882, 1975.

Bernhardt, P. A., R. A. Roussel-Dupre, M. B. Pongratz, G. Haerendel, A. Valenzuela, D. A. Gurnett, and R. R. Anderson, Observations and theory of the AMPTE magnetotail barium releases, *J. Geophys. Res., 92*, 5777, 1987.

Brecht, S. H., Dispersion relations for ion waves with finite parallel wavelengths in plasmas of finite beta, *J. Plasma Phys., 27*, 351, 1982.

Drake, J. F., and T. T. Lee, Irreversibility and transport in the lower hybrid drift instability, *Phys. Fluids, 24*, 1115, 1981.

Drake, J. F., P. N. Guzdar, A. B. Hassam, and J. D. Huba, Nonlinear mode coupling theory of the lower hybrid drift instability, *Phys. Fluids, 27*, 1147, 1984.

Forslund, D. W., R. L. Morse, and C. W. Nielson, Electron cyclotron drift instability, *Phys. Rev. Lett., 25*, 1266, 1970.

Galvez, M., S. P. Gary, C. Barnes, and D. Winske, Computer simulations of plasma expansion across a magnetic field, *Phys. Fluids*, submitted, 1987.

Gurnett, D. A., R. R. Anderson, P. A. Bernhardt, H. Luhr, G. Haerendel, O. H. Bauer, H. C. Koons, and R. H. Holzworth, Plasma waves associated with the first AMPTE magnetotail barium release, *Geophys. Res. Lett., 13*, 644, 1986.

Hassam, A. B., and J. D. Huba, Structuring in the AMPTE magnetotail barium releases, *Geophys. Res. Lett., 14*, 60, 1987.

Huba, J. D., Onset conditions for structure in magnetically confined plasma expansions, NRL Memo Report XXX, 1987.

Huba, J. D., J. G. Lyon, and A. B. Hassam, Theory and simulation of the Rayleigh Taylor instability in the large Larmor radius limit, *Phys. Rev. Lett.*, submitted, 1987.

Keilhacker, M., M. Kornherr, H. Niedermeyer, F. Soldner, and K. -H. Steuer, Flute instabilities during fast magnetic compression of collisionless $\beta = 1$ plasmas, *Phys. Rev. Lett., 32*, 1044, 1974.

Lampe, M., W. M. Manheimer, J. B. McBride, J. H. Orens, K. Papadopoulos, R. Shanny, and R. N. Sudan, Theory and simulation of the beam cyclotron instability, *Phys. Fluids, 15*, 662, 1972.

Lashmore-Davies, C. N., and T. J. Martin, Electrostatic instabilities driven by an electric current perpendicular to a magnetic field, *Nucl. Fusion, 13*, 193, 1973.

Okada, S., K. Sato, and T. Sekiguchi, Behavior of laser produced plasma in a uniform magnetic field–plasma instabilities, *Japan J. Appl. Phys., 20*, 157, 1981.

Ripin, B. H., E. A. McLean, C. K. Manka, C. Pawley, J. A. Stamper, T. A. Peyser, A. N. Mostovych, J. Grun, A. B. Hassam, and J. D. Huba, Large Larmor radius interchange instability, *Phys. Rev. Lett., 59*, 2299, 1987.

Shonk, C. R. and R. L. Morse, Two dimensional simulation of shock waves in collisionless plasmas, in Proceedings of the Second Conference on Plasma Simulation, 1968.

Winske, D., and P. C. Liewer, Particle simulation studies of the lower hybrid drift instability, *Phys. Fluids, 21*, 1017, 1978.

Winske, D., The lower hybrid drift instability as source of surface modes on AMPTE barium magnetotail releases, *J. Geophys. Res.*, in press, 1987.

Table 1. Simulation parameters for runs with various cell sizes.

	(A)		(B)		(C)	
$\Delta(c/\omega_e)$		0.125		0.0625		0.03125
$\omega_e t$	25	50	25	50	25	50
$n_e v_\theta / n_o c$	0.22	0.25	0.23	0.25	0.30	0.25
n_e/n_o	15	10	15	10	16	10
v_θ/c	0.015	0.025	0.015	0.025	0.017	0.025
v_θ(phase sp.)	0.015	0.025	0.2	0.025	0.2	0.025
V_g/v_A	1.6	2.4	1.6	2.4	1.7	2.4
$k_{LHD}c/\omega_e$	10.5	8.0	10.5	8.0	10.5	8.0
$r(c/\omega_e)$	1.5	2.0	1.5	2.0	1.5	2.0
$m_{LHD} = kr$	16	16	16	16	16	16
$m_{num} = r/\Delta$	12	16	24	32	48	64

Other parameters: $\Omega_e/\omega_e = 0.2$, $T_e/T_i = 1$, $m_i/m_e = 100$, $v_e/c = 0.01$, and $\epsilon_n c/\omega_e = 10$.

Figure Captions

Figure 1. Example of plasma structuring observed in the NRL laser [Ripin *et al.*, unpublished].

Figure 2. Instability mechanism.

Figure 3. Simulation of the instability, showing the ions in real space at various times.

Figure 4. Ion density contours from various simulations to test mass scaling of the wavelength.

Figure 5. Ion density contours from various simulations to test Ω_e/ω_e scaling of the wavelength.

Figure 6. Ion density contours from various simulations to test scaling of the wavelength, varying m_i/m_e and Ω_e/ω_e to keep R_B constant.

Figure 7. Ion density contours from various simulations to test scaling of the wavelength, varying V_D/c and Ω_e/ω_e to keep R_B constant.

Figure 8. Comparison of simulations with different initial velocity distributions: [top] $V_r = V_D$(constant), [bottom] $V_r = \sqrt{2}V_D r/r_o$.

Figure 9. Comparison of simulations with different angular spread ($\pm\theta_o$): $\theta_o = 180^o, 90^o, 45^o$ with $V_r = V_D r/r_o$ and $\theta_o = 90^o$ with $V_r = V_D$.

Figure 10. Simulations at various times (in reverse order) showing Y-shaped structure at top is not bifurcating.

Figure 11. Simulation at various times showing arms bend in the electron sense of rotation.

Figure 12. Simulation at various times showing persistence and propagation of coherent density clumps.

Figure 13. Results of simulations showing the effect of varying cell size: ion density

contours at various times for (A) $\Delta x = 0.125c/\omega_e$, (B) 0.0625, and (C) 0.03125. (The standard case has $\Delta x = 0.2$).

Figure 14. Results of linear theory for the simulation parameters of the standard case showing the growth rate as a function of k for the LHDI and the first two harmonics of the ECDI.

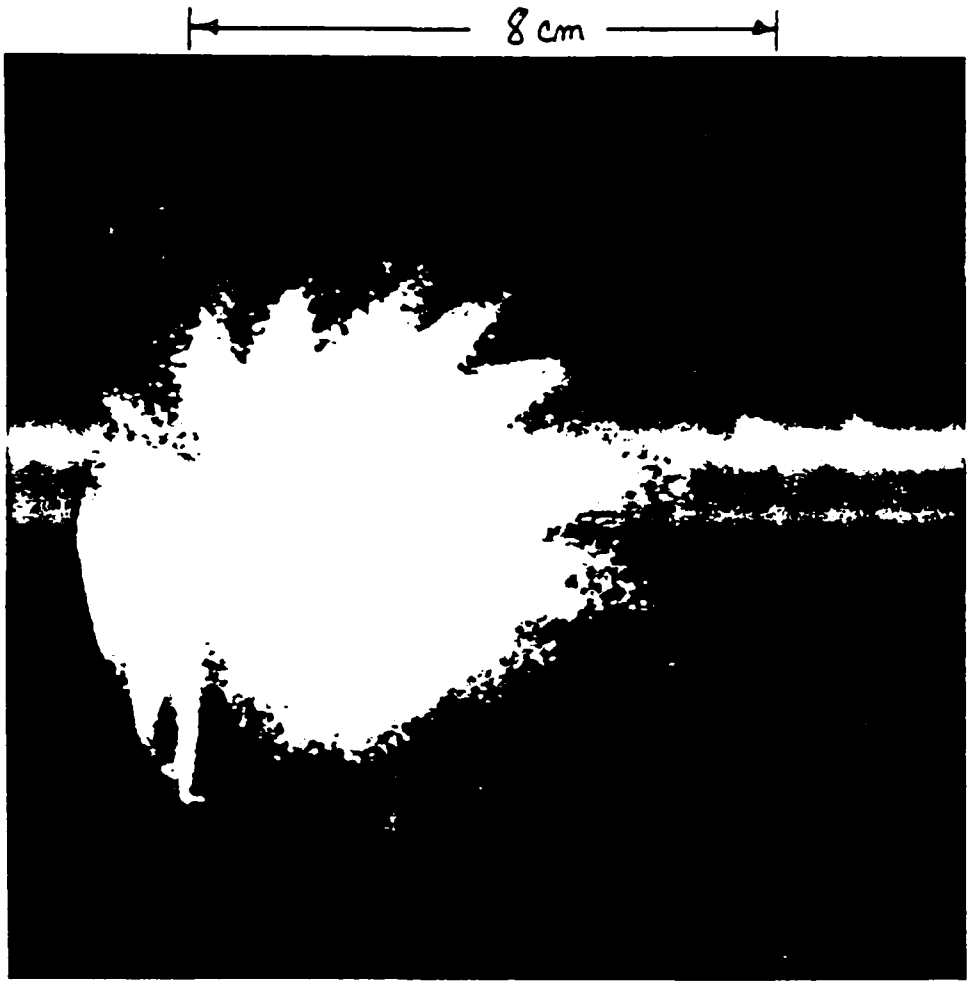

Figure 1

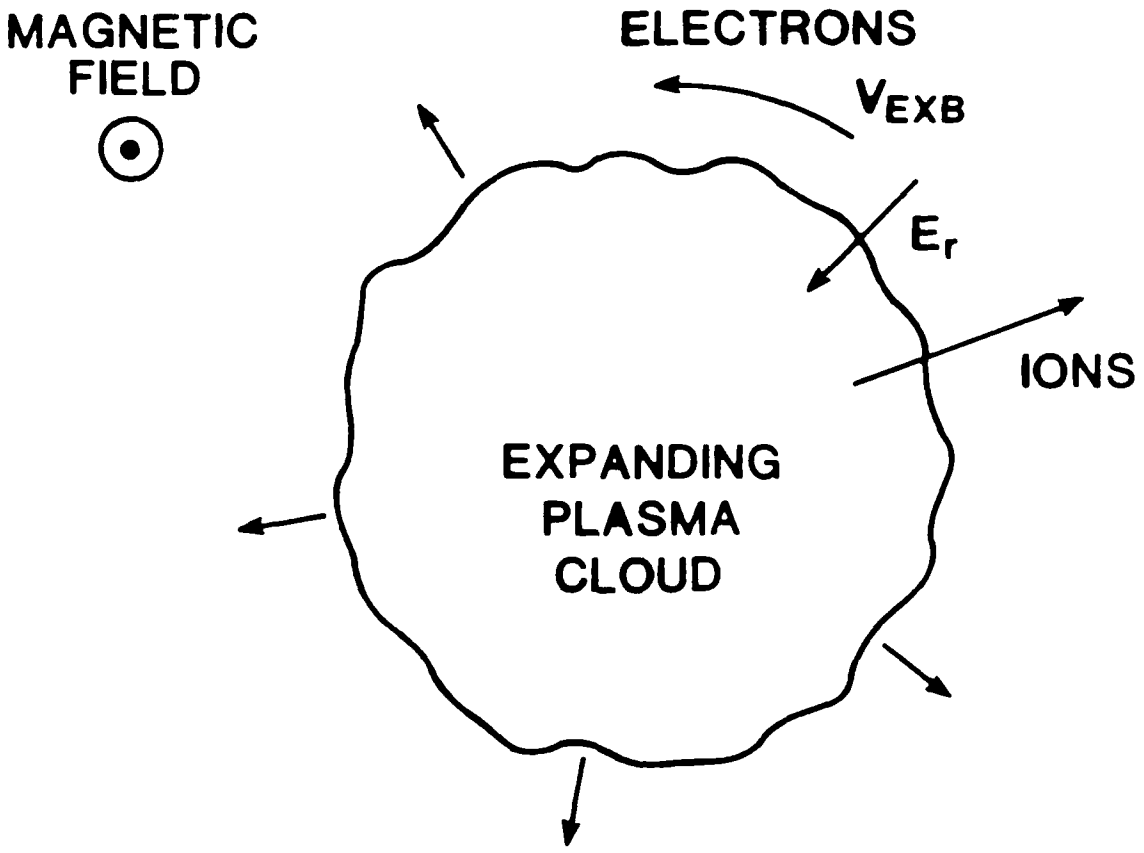
MAGNETIC
FIELD
ELECTRONS
V_{EXB}
E_r
IONS
EXPANDING
PLASMA
CLOUD

Figure 2

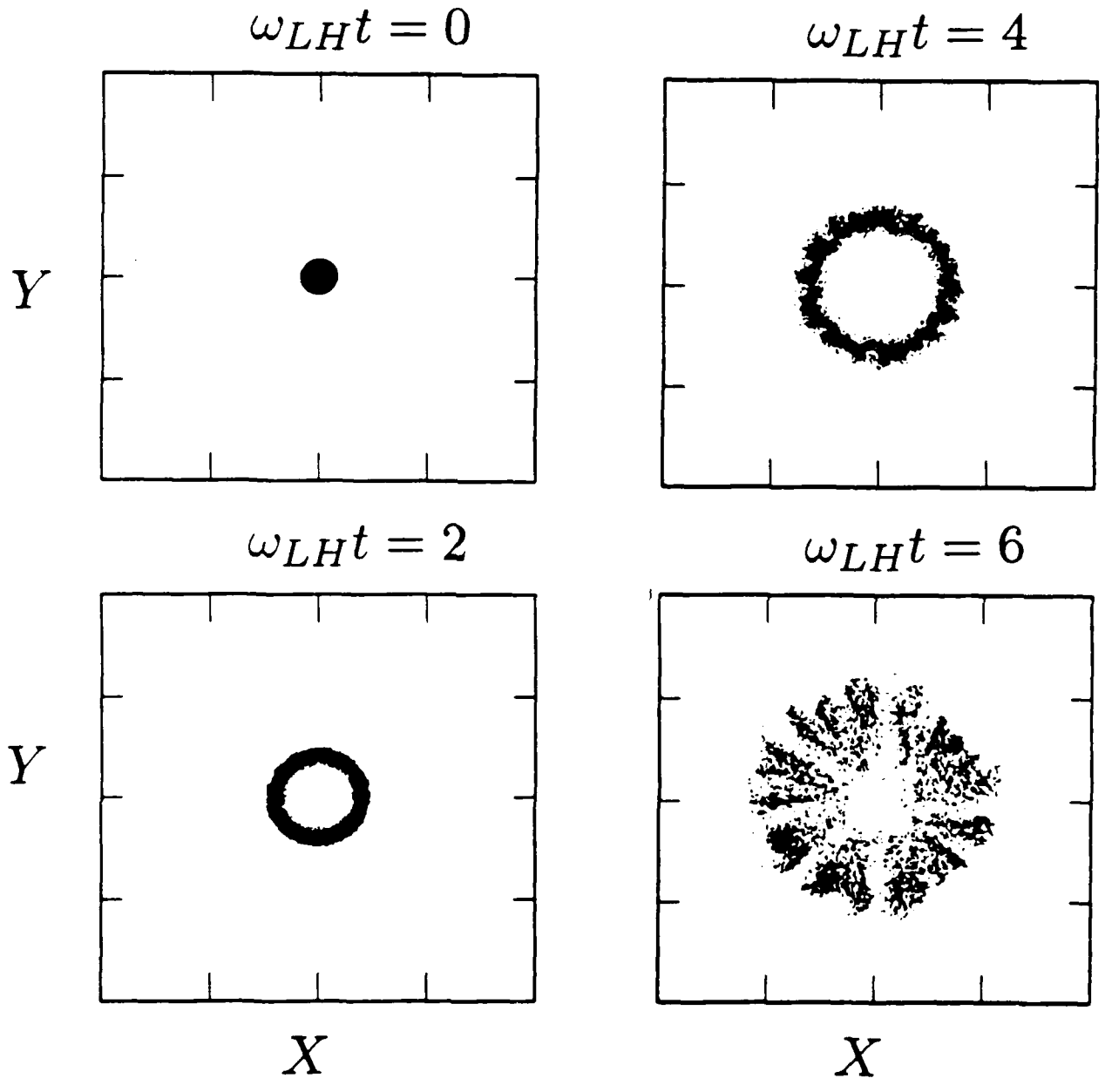

Figure 3

$m_i/m_e = 25$ $\omega_e t = 175$

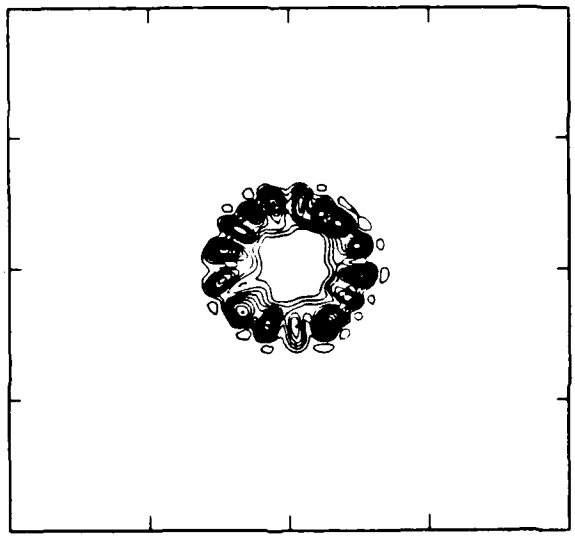

$m_i/m_e = 100$ $\omega_e t = 225$

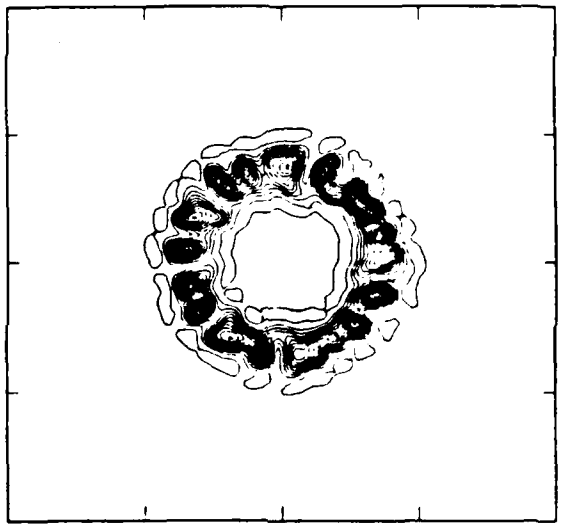

$m_i/m_e = 400$ $\omega_e t = 300$

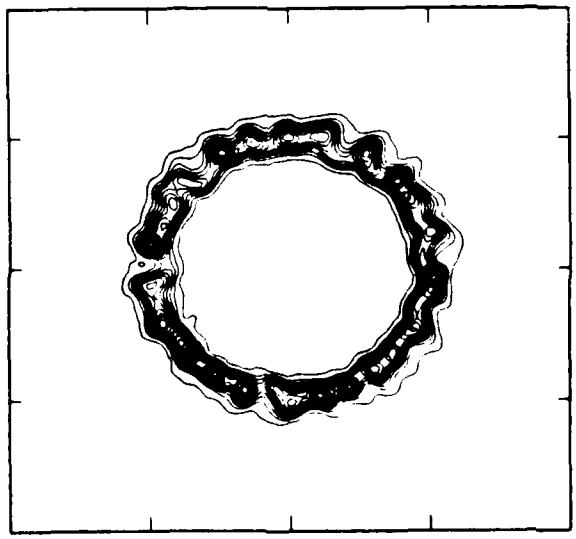

Figure 4

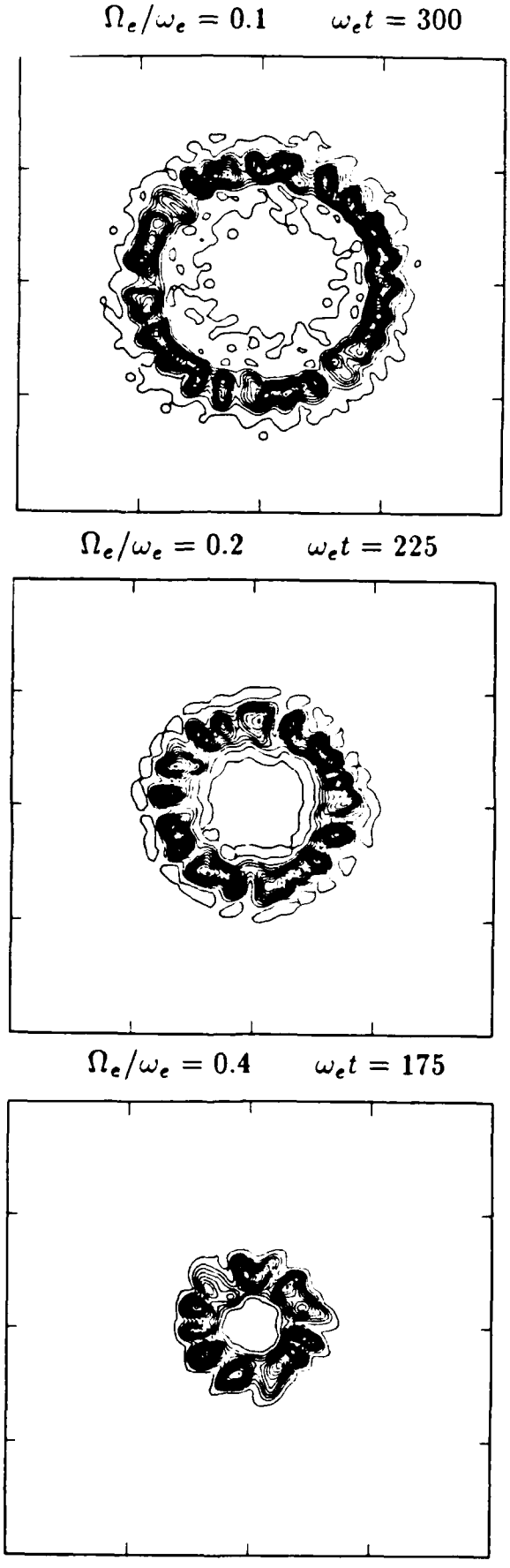
$\Omega_e/\omega_e = 0.1$ $\omega_e t = 300$
$\Omega_e/\omega_e = 0.2$ $\omega_e t = 225$
$\Omega_e/\omega_e = 0.4$ $\omega_e t = 175$

Figure 5

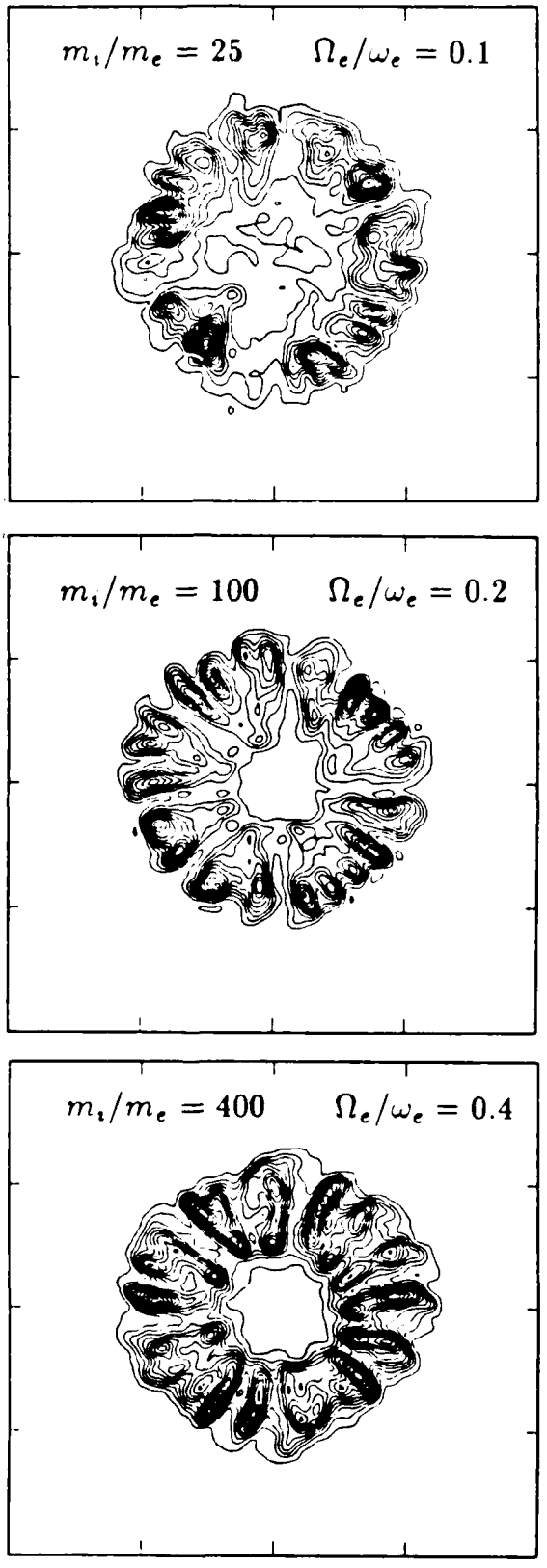
$m_i/m_e = 25$ $\Omega_e/\omega_e = 0.1$
$m_i/m_e = 100$ $\Omega_e/\omega_e = 0.2$
$m_i/m_e = 400$ $\Omega_e/\omega_e = 0.4$

Figure 6

$\Omega_e/\omega_e = 0.1 \qquad V_D/c = 0.01 \qquad \omega_e t = 500$

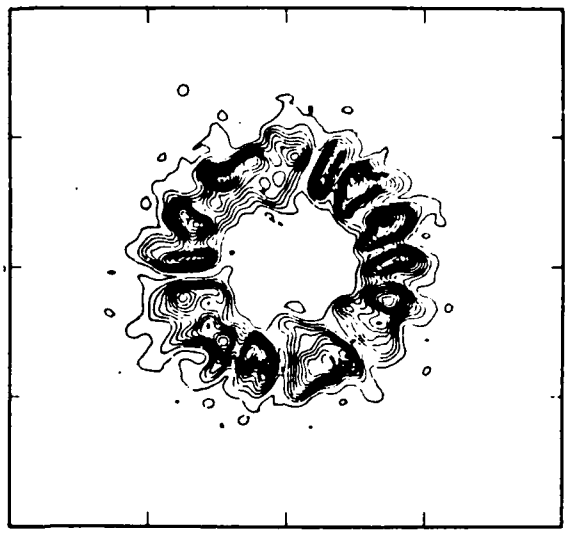

$\Omega_e/\omega_e = 0.2 \qquad V_D/c = 0.02 \qquad \omega_e t = 300$

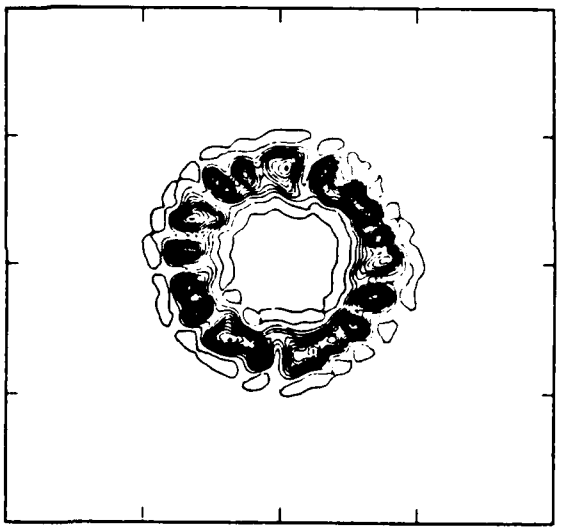

$\Omega_e/\omega_e = 0.4 \qquad V_D/c = 0.04 \qquad \omega_e t = 150$

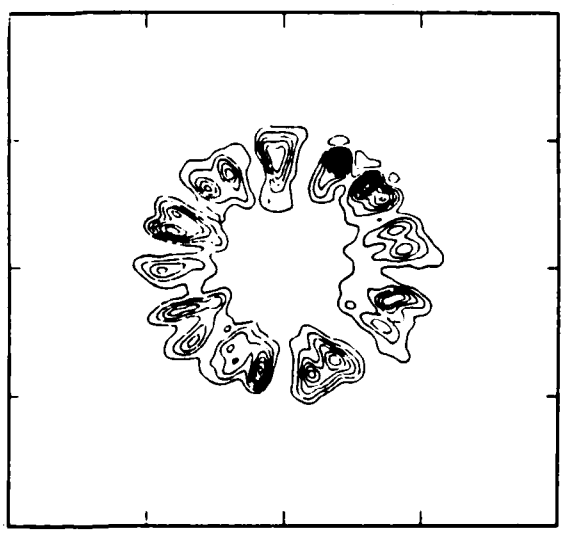

Figure 7

$V_r = V_o$

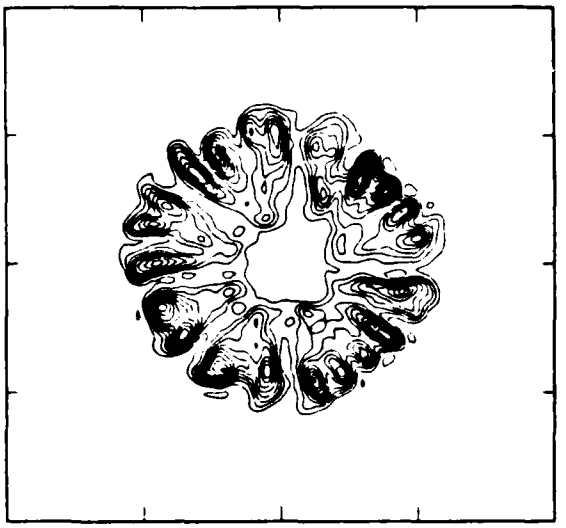

$V_r = \sqrt{2r}V_o$

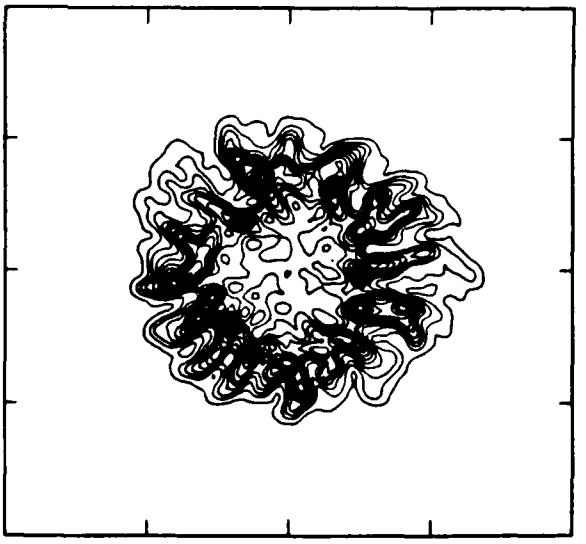

Figure 8

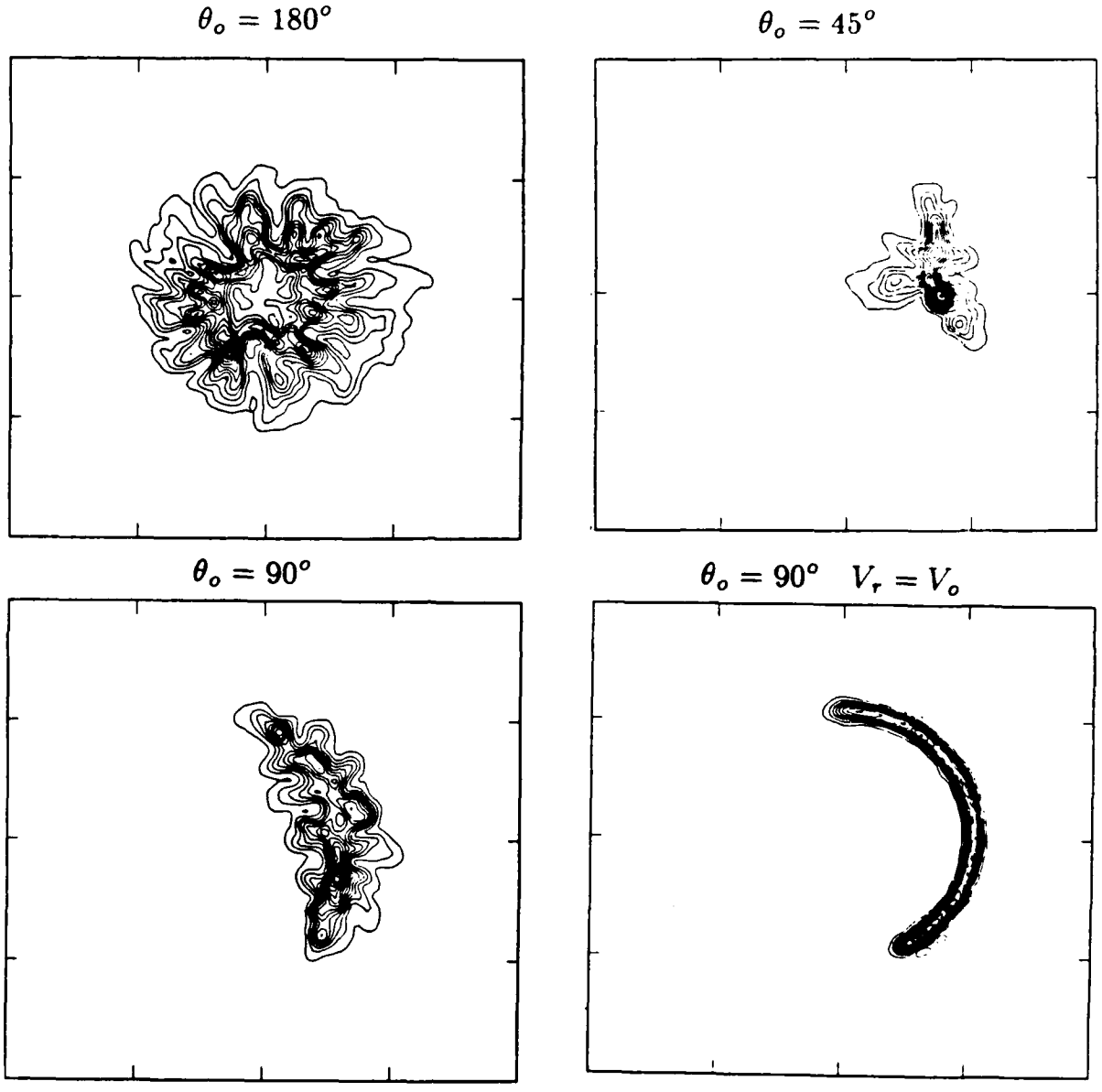

Figure 9

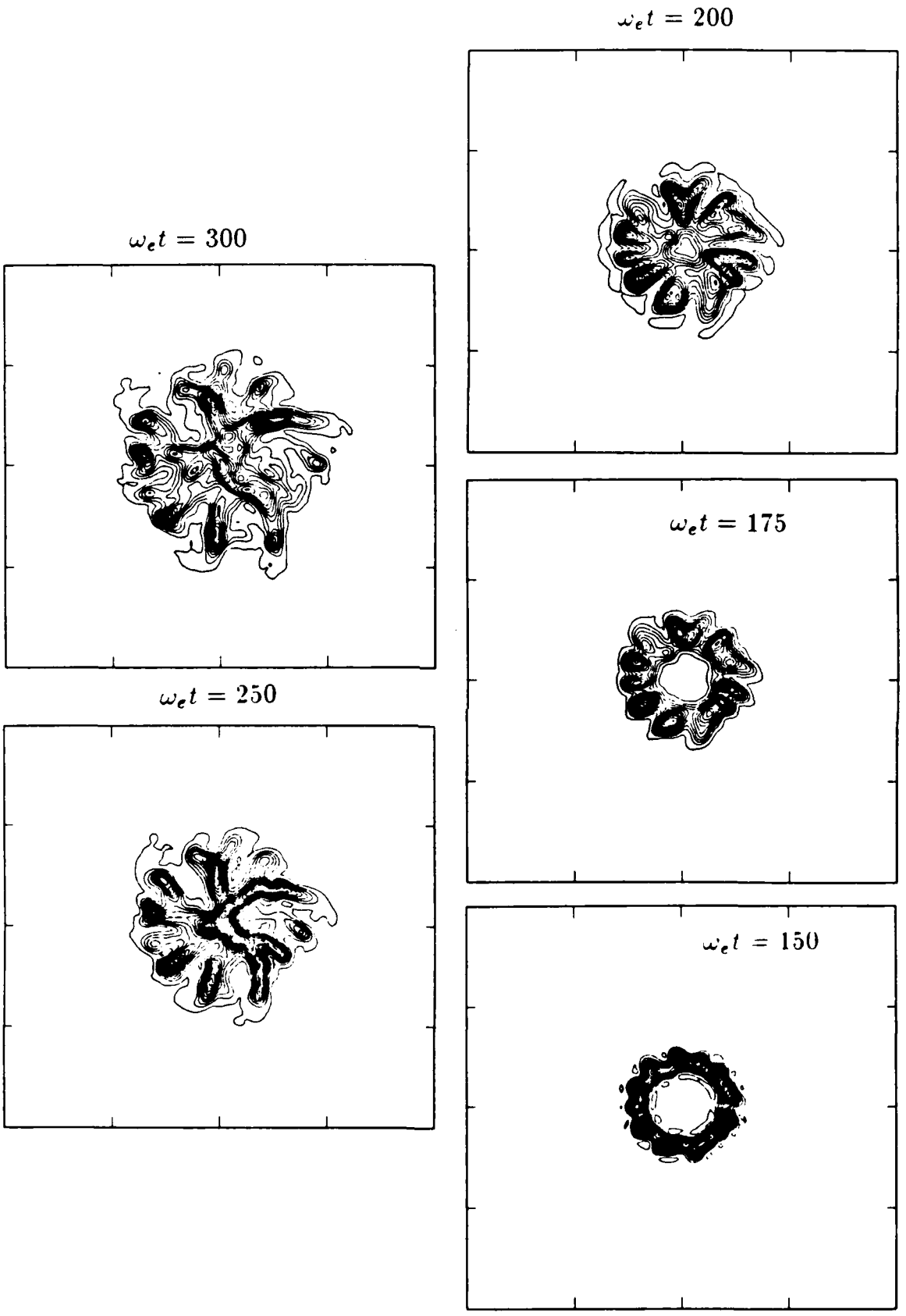
$\omega_e t = 200$
$\omega_e t = 300$
$\omega_e t = 175$
$\omega_e t = 250$
$\omega_e t = 150$

Figure 10

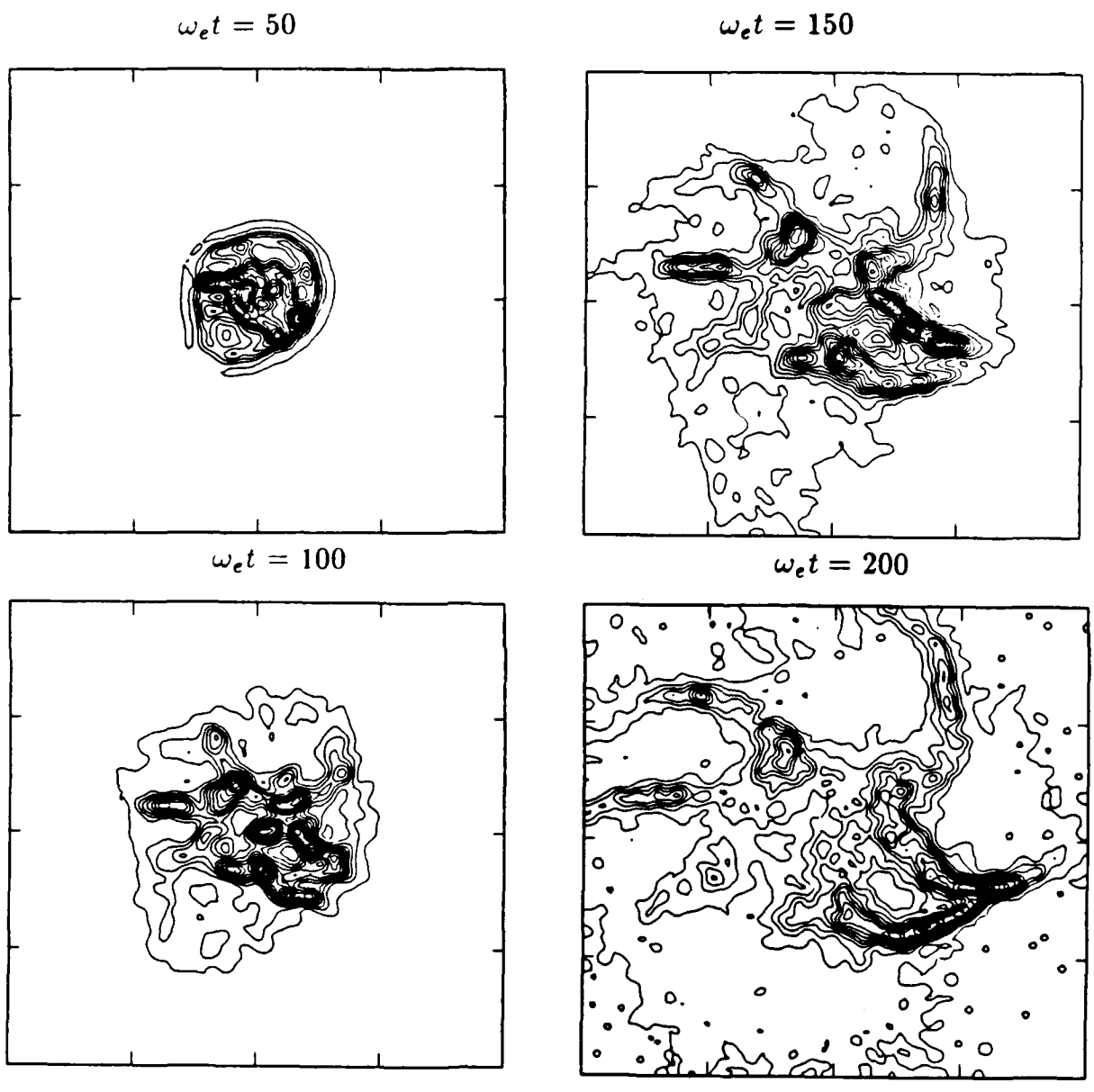

Figure 11

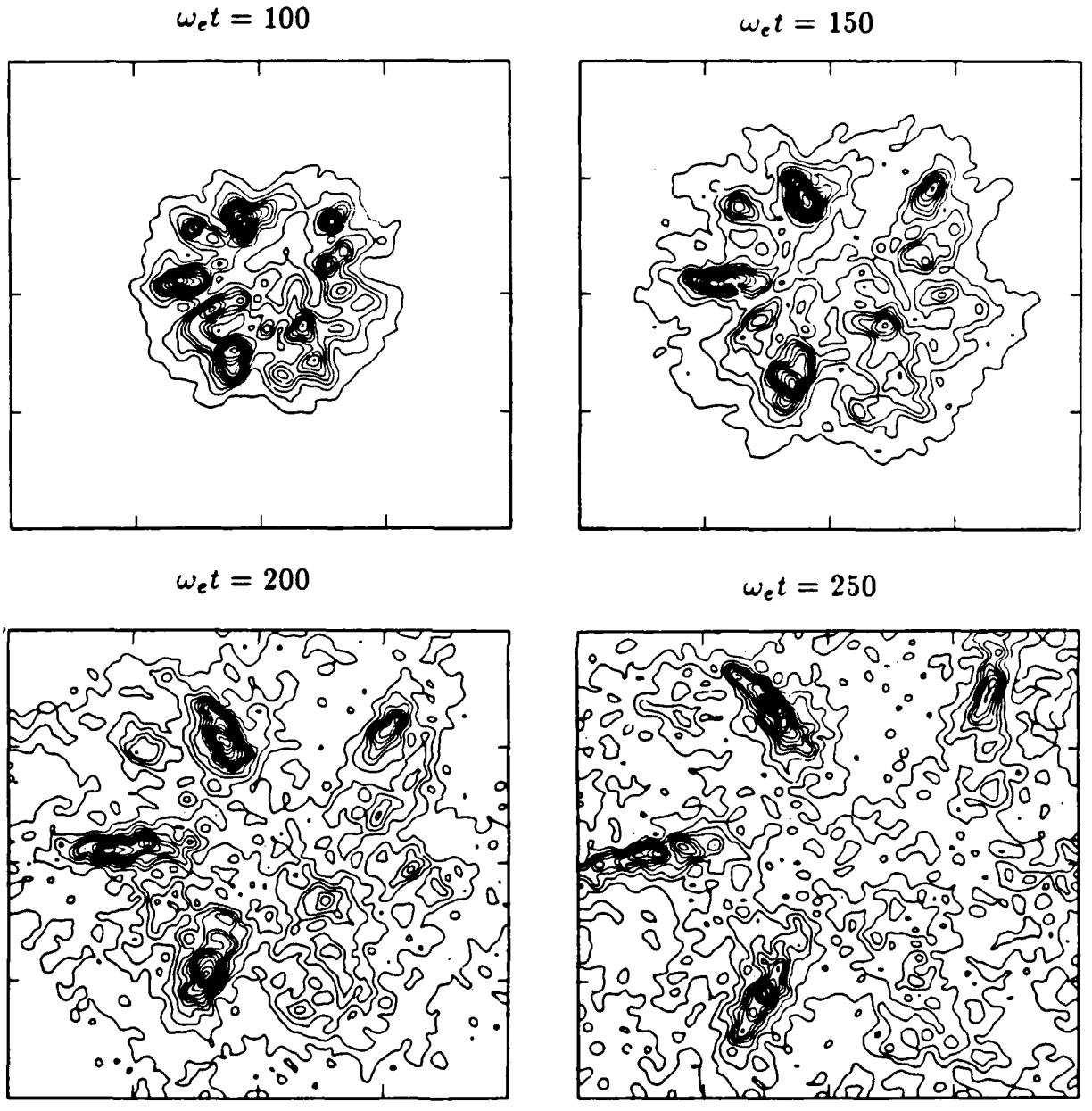

Figure 12

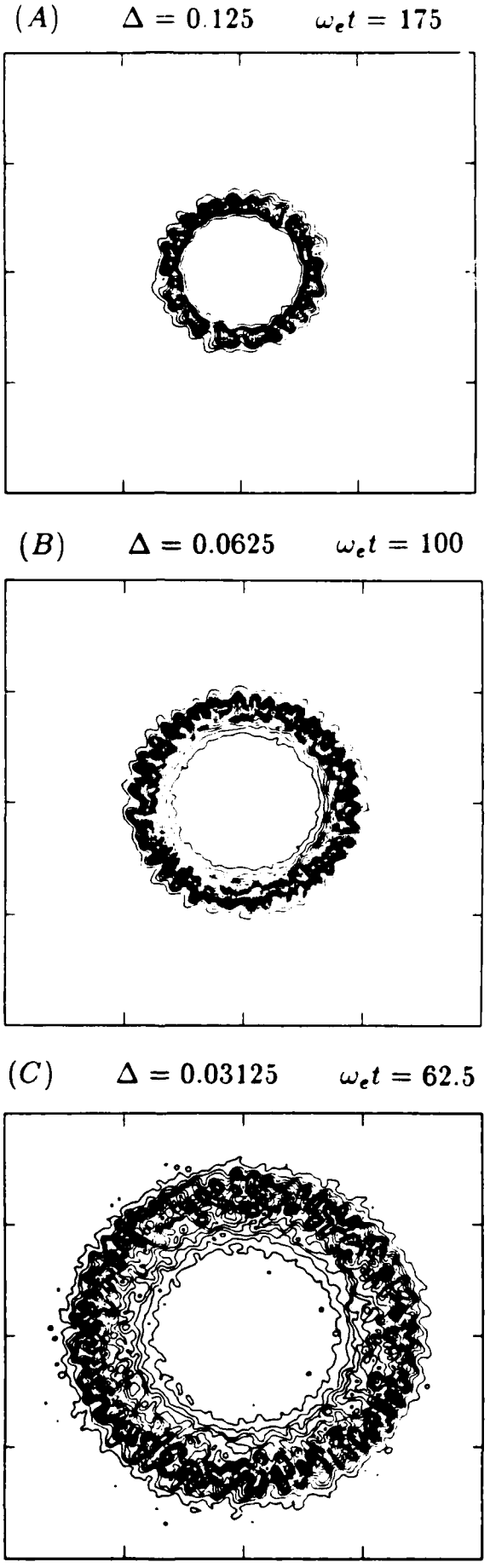

Figure 13

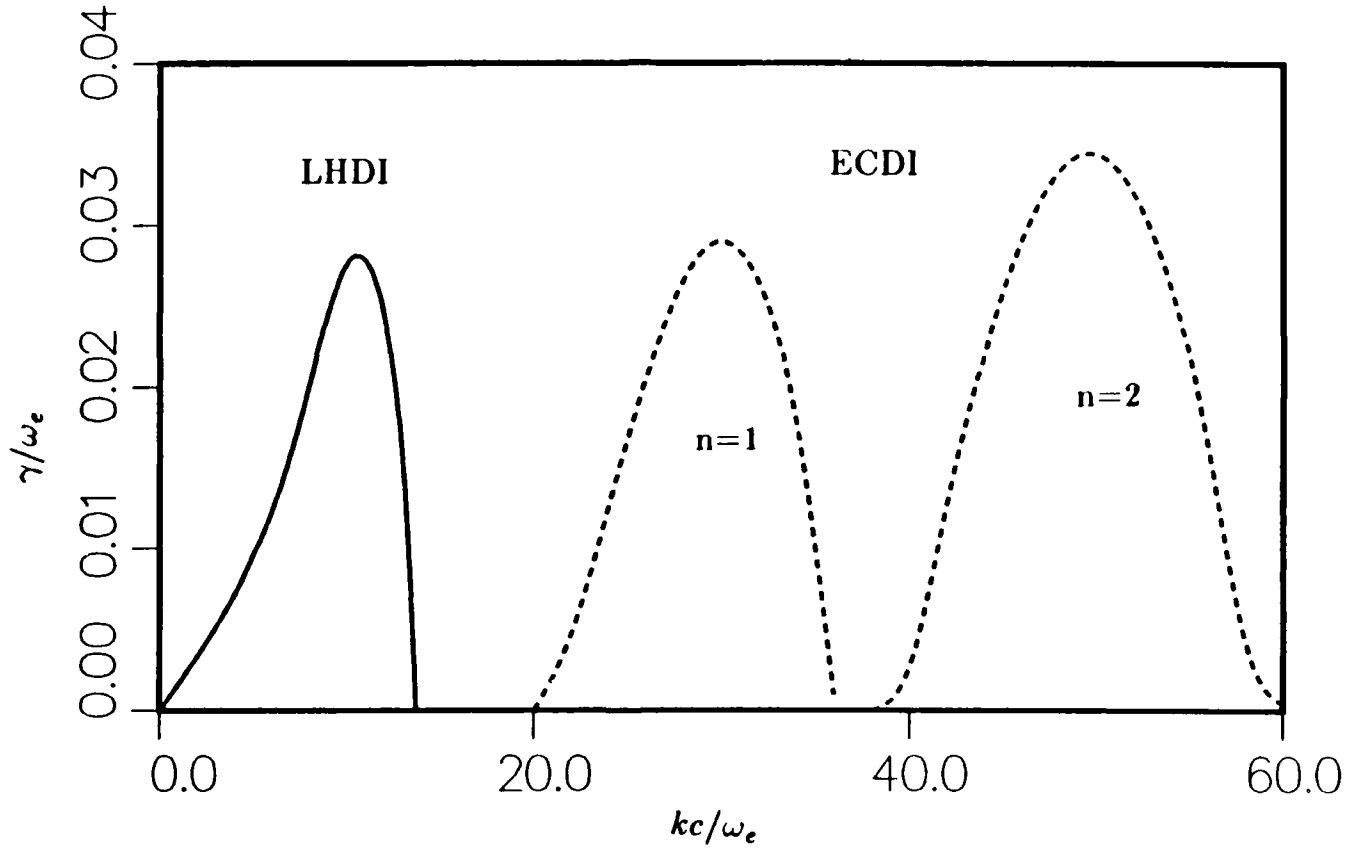
LHDI
ECDI
n=1
n=2
0.00
0.01
0.02
0.03
0.04
γ/ω_e
0.0
20.0
40.0
60.0
kc/ω_e

Figure 14

DISTRIBUTION

Dr. B. H. Ripin
Code 4732
Naval Res. Lab.
Washington, DC 20375

Dr. E. McLean
Code 4732
Naval Res. Lab.
Washington, DC 20375

Dr. J. Stamper
Code 4732
Naval Res. Lab.
Washington, DC 20375

Dr. Paul Bernhardt
Code 4780
Naval Res. Lab.
Washington, DC 20375

Dr. Walter Chesnut
SRI International
333 Ravenswood Ave.
Menlo Park, CA 94025

Dr. J. L. Sperling
JAYCOR
11011 Torreyana Road
P. O. Box 85154
San Diego, CA 92138

Dr. R. Stellingwerf
Mission Research Corp.
1720 Randolph Rd. S. E.
Albuquerque, NM 87106

Dr. R. Peterkin
Mission Research Corp.
1720 Randolph Rd. S. E.
Albuquerque, NM 87106

Dr. K. Hain
Maxwell S-Cubed Div.
1800 Diagonal Rd.
Alexandria, VA 22314

Dr E. Hyman
SAIC
1710 Goodridge Dr.
McLean, VA 22102

Dr J. Guillory
PRC
5850 Leesburg Pike # 23
Falls Church, VA 22041

Dr. L. Wittwer
RAAE
Defense Nuclear Agency
Washington, DC 20305

Dr. B. Prasad
RAAE
Defense Nuclear Agency
Washington, DC 20305

Director [2]
Attn: STTI
Defense Nuclear Agency
Washington, DC 20305-1000

Dr. R. W. Kilb
Mission Research Corp.
P. O. Box 719
Santa Barbara, CA 93102

Dr. W. W. White
Mission Research Corp.
P. O. Box 719
Santa Barbara, CA 93102

Dr. M. Hausman
Mission Research Corp.
P. O. Box 719
Santa Barbara, CA 93102

Dr. D. Sowle
Mission Research Corp.
P. O. Box 719
Santa Barbara, CA 93102

Prof. D. Papadopoulos
Astronomy Program
University of Maryland
College Park, MD 20742

Dr. J. D. Huba
Code 4780
Naval Res. Lab.
Washington, DC 20375

Dr. J. Lyon
Code 4780
Naval Res. Lab.
Washington, DC 20375

Dr. J. Giuliani
Code 4780
Naval Res. Lab.
Washington, DC 20375

Dr S. Brecht
Berkeley Research Associates
P.O. Box 241
Berkeley, CA 94701

Dr V. Thomas
Berkeley Research Associates
P.O. Box 241
Berkeley, CA 94701

Dr. H. Carl Fitz
Physical Research, Inc.
134 Holiday Ct., Suite 309
Annapolis, MD 21401

Dr. R. Armstrong
Mission Research Corp.
One Tara Blvd. Suite 302
Nashua, NH 03062

Defense Technical Information Center [2]
Cameron Station
Alexandrai, VA 22314

Dr. R. Henderson, W385
Director, JASON Program Office
The MITRE Corp.
7525 Colshire Dr.
McLeam, VA 22102

DASIAC
815 State St.
P.O. Drawer QQ
Santa Barbara, CA 93102

Dr. J. Kindel
MRC
127 Eastgate #20800
Los Alamos, NM 87544

Dr. T. Mazurek
Mission Research Corp.
P. O. Box 719
Santa Barbara, CA 93102

Dr. C. Longmire
Mission Research Corp.
P. O. Box 719
Santa Barbara, CA 93102

Dr. E. Witt
Mission Research Corp.
P. O. Box 719
Santa Barbara, CA 93102

Dr. J. R. Thompson
Austin Research Associates
1901 Rutland Dr.
Austin, TX 78758

Dr. J. M. Cornwall
Dept. of Physics
UCLA
Los Angeles, CA 90024

Dr. D. Hammer
Laboratory for Plasma Studies
309 Upson Hall
Cornell University
Ithaca, NY 14853

Dr. C. Prettie
Berkeley Research Associates
P.O. Box 241
Berkeley, CA 94701

Dr. J. Workman
Berkeley Research Associates
P.O. Box 241
Berkeley, CA 94701

Dr. D. Simons
ESS-7
MS D466

Dr. D. Sappenfield
ESS-7
MS D466

Dr. G. Smith
ESS-DOT
MS D446

Dr. M. Pongratz
ESS-DOT
MS D446

END

DATE

FILMED

5-88

DTIC